UNIVERSITY OF CALIFORNIA
SANTA CRUZ

AN ADAPTIVE FRAMEWORK FOR IMAGE AND VIDEO SENSING

A thesis submitted in partial satisfaction of the
requirements for the degree of

MASTER OF SCIENCE

in

ELECTRICAL ENGINEERING

by

Lior Zimet

March 2005

The Thesis of Lior Zimet
is approved:

Professor Peyman Milanfar, Chair

Professor Ali Shakouri

Professor Hai Tao

Robert C. Miller
Vice Chancellor for Research and
Dean of Graduate Studies

Contents

List of Figures

Abstract

An Adaptive Framework for Image and Video Sensing

by

Lior Zimet

Current digital imaging devices often enable the user to capture still frames at a high spatial resolution, or a short video clip at a lower spatial resolution. With bandwidth limitations inherent to any sensor, there is clearly a tradeoff between spatial and temporal sampling rates, which present-day sensors do not exploit. The fixed sampling rate that is normally used does not capture the scene according to its content and artifacts such as aliasing and motion blur appear. Moreover, the available bandwidth on the camera transmission or memory is not optimally utilized. In this paper we outline a framework for an adaptive sensor where the spatial and temporal sampling rates are adapted to the scene. The sensor is adjusted to capture the scene with respect to its content. In the adaptation process, the spatial and temporal content of the video sequence are measured to evaluate the required sampling rate. We propose a robust, computationally inexpensive, content measure that works in the spatio-temporal domain as opposed to the traditional frequency domain methods. We show that the measure is accurate and robust in the presence of noise and aliasing. The varying sampling rate stream captures the scene more efficiently and with fewer artifacts such that in a post-processing step an enhanced resolution sequence can be effectively composed or an overall lower bandwidth can be realized, with small distortion.

To my wife Miriam Sivan-Zimet and my son Yoav

Acknowledgements

I would like to express my gratitude to my advisor Prof. Peyman Milanfar for guiding me throughout this work, supporting my ideas, and introducing me to the world of research. His invaluable suggestions helped me to seek the right direction in this research. I also thank my other committee members Prof. Ali Shakouri and Prof. Hai Tao for their review and comments.

Special thanks to my colleagues at the Multi-Dimensional Signal Processing (MDSP) group Sina Farsiu, Dirk Robinson, and Amyn Poonawala and especially Morteza Shahram for fruitful discussions and collaboration.

I wish to thank my friend Tamar Kariv for her great support with software development and advise. I also wish to thank Steven Brook, my manger at Zoran corporation, for for his support in my studies and for the flexibility he gave me at work in order to pursue this MS degree.

Above all, the love, care, patience, and support of my wife Miri and my son Yoav. Nothing would have happened without them!

Santa Cruz, CA March 18, 2005 Lior Zimet

Chapter 1

Introduction

In this chapter we introduce the adaptive imaging framework. We provide a brief description of the imaging sensor spatio-temporal characteristics and show how it can be used to capture the scene more effectively. We show possible sensor architectures and provide the general description for an adaptive sensor operation. Finally, we list related works and the thesis organization.

1.1 The Imaging Sensor Spatio-Temporal Characteristics

Imaging devices have limited spatial and temporal resolution. An image is formed when light energy is integrated by an image sensor over a time interval. The minimum energy level for the light to be detected by the sensor is determined by signal to noise ratio characteristics of the detector [5]. Therefore, the exposure time required to ensure detection of light is inversely proportional to the area of the pixel. In other

words, exposure time is proportional to spatial resolution. This is the fundamental trade off between the spatial sampling (number of pixels) and the temporal sampling (number of images per second). Other parameters such as readout and analog to digital conversion time as well as sensor circuit timing have second order effects on the spatio-temporal trade-off. Figure 1.1 is an example of the spatio-temporal sampling rate tradeoff in a typical camera (e.g. PixeLINK PL-A661). The markers along the graph are typical sampling rates used by digital image sensors for different applications. The parameters of the trade-off line are determined by the characteristics of the materials used by the detector and the light energy level. A conventional video camera has a typical temporal sampling rate of 30 frame per second (fps) and a spatial sampling rate of 720×480 pixels, whereas a typical still digital camera has spatial resolution of 2048×1536 pixels.

The minimal size of spatial features or objects that can be visually detected in an image is determined by the spatial sampling rate and the camera-induced blur. The maximal speed of dynamic events that can be observed in a video sequence is determined by the temporal sampling rate [14]. We define the sensor operating point as the pair of {spatial sampling rate, temporal sampling rate} at which the sensor is operating.

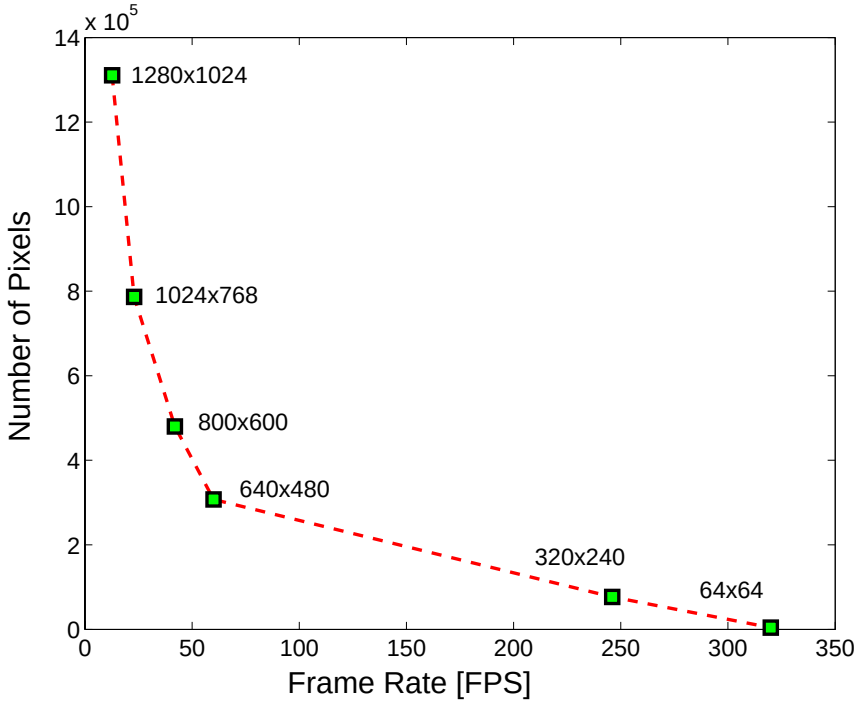

Figure 1.1: Typical tradeoff of spatial vs. temporal sampling in imaging sensor

1.2 Adaptive Versus Non-Adaptive Image Sensing

A non-adaptive sensor is normally set to a fixed operating point, which does not depend on the scene. Therefore, the data from the sensor can be spatially or temporally aliased due to insufficient sampling rate. Insufficient temporal sampling rate introduces motion based aliasing. Motion aliasing occurs when the trajectory generated by a fast moving object is characterized by frequencies which are higher than the temporal sampling rate of the sensor. In this case, the high temporal frequencies are folded into the low temporal frequencies. The observable result is a distorted or even false trajectory of the moving object [14] (e.g. wheels on a fast-moving cart appearing to rotate backwards in a film captured at typical video rate). Meanwhile,

insufficient spatial sampling rate will remove details from the image and introduce visual effects such as blur and aliasing.

Now, instead of relying on a single point on the spatio-temporal tradeoff curve (Figure 1.1), we could adapt the sensor to run at an operating point that is determined by the scene. An adaptive sensor would have the ability to change its operating point according to a measure of the temporal and spatial content in the scene. It therefore captures the scene more accurately and more efficiently with the available bit-rate or sensor memory or communication capabilities. The design of such a novel sensor can also be informed by user preferences in terms of acceptable levels of spatial or temporal aliasing or other factors. Figure 1.2 is an illustration of the sampling difference between an adaptive and non-adaptive imaging sensor. A Block diagram of an adaptive sensor is shown in Figure 1.3.

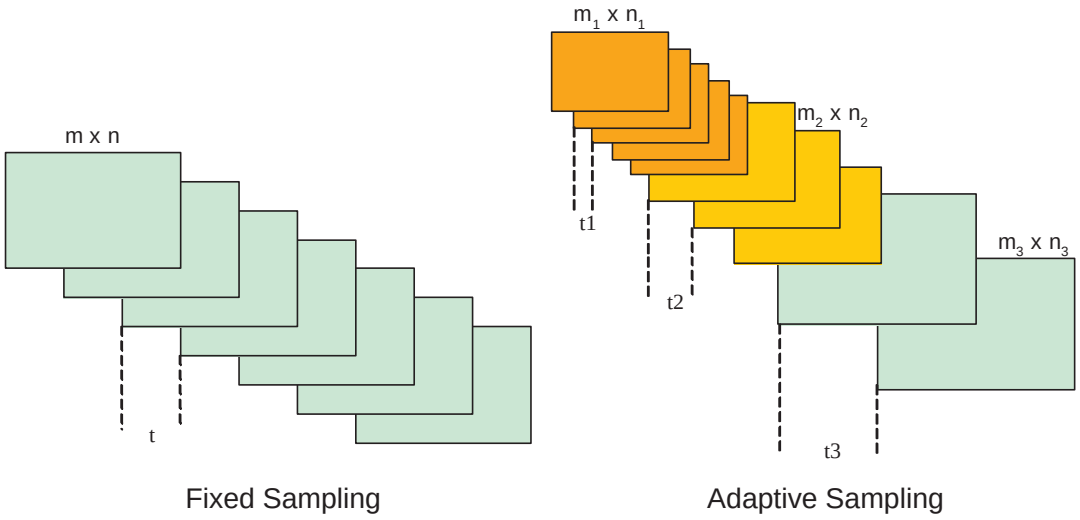

Figure 1.2: Adaptive versus non-adaptive sampling

The spatial and temporal dimensions are very different in nature, yet are

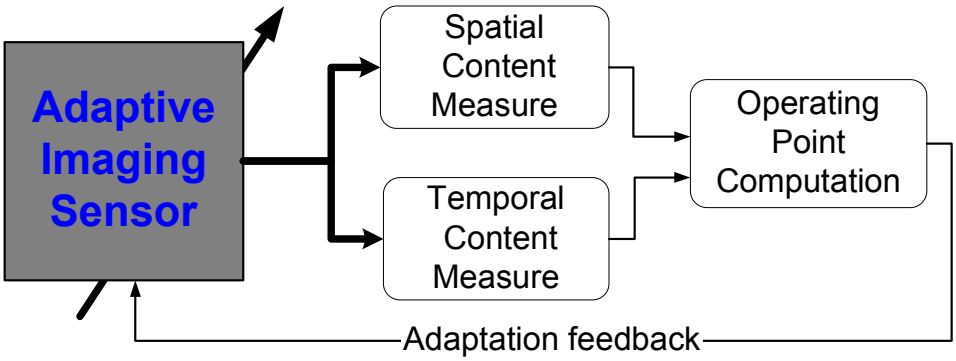

Figure 1.3: An adaptive sensor block diagram

inter-related through the sensors capabilities. In the proposed adaptive sensor architecture we measure the spatial and temporal content separately to determine the required sampling rate for the current scene. We develop a robust, computationally inexpensive, measure for the scene content. The measure works in the spatio-temporal domain as opposed to the traditional frequency domain. We show that the measure is usable in the presence of noise and aliasing. Section 2 of the paper describes the content measure along with other possible methods.

In the single sensor architecture as shown in Figure 1.3, the content measure is computed on the same data that the sensor is capturing at different operating points. Therefore, the accuracy of the spatial and temporal content measures depends on the operating point. Higher sampling will result in a more accurate measure and vice versa. An optional architecture would be a three-sensor configuration as depicted

in Figure 1.4. Here we dedicate a high frame rate, low spatial resolution sensor for the temporal content measure and a low frame rate high spatial resolution sensor for the spatial content measure. The scene capture is done through a third sensor that has variable spatio-temporal sampling capabilities. Although this architecture provides more accurate measure for the scene content it is less applicable in practice and imposes other issues such as three-way optical beam splitting and circuit complexity. As further described in Chapter 4, in single sensor architecture the content measure is compromised only in the transitions between operating points and the system convergence to correct operating point is guaranteed.

The adaptive sensor measures the scene content continuously for every incoming frame. The required sampling rate is then determined from this measure. The required sampling rate can sometimes be out of the sensor's capabilities and a projection to the nearest possible operating point in the sensor's operating space is required. The conversion from the content measure to sensor operating point is discussed in Chapter 3. Using a feedback loop the sensor is reconfigured to the new operating point.

Another important aspect of a sensor's capability is the data transmission bandwidth at its output. A fixed sampling rate of the sensor determines a fixed bit-rate at the output assuming no compression involved. But in many cases such as static scenes or scenes with very little details the said bandwidth is not utilized efficiently. In the adaptive framework, the sensor determines the required sampling rate and can therefore either reduce the bit-rate to the minimum necessary, or use

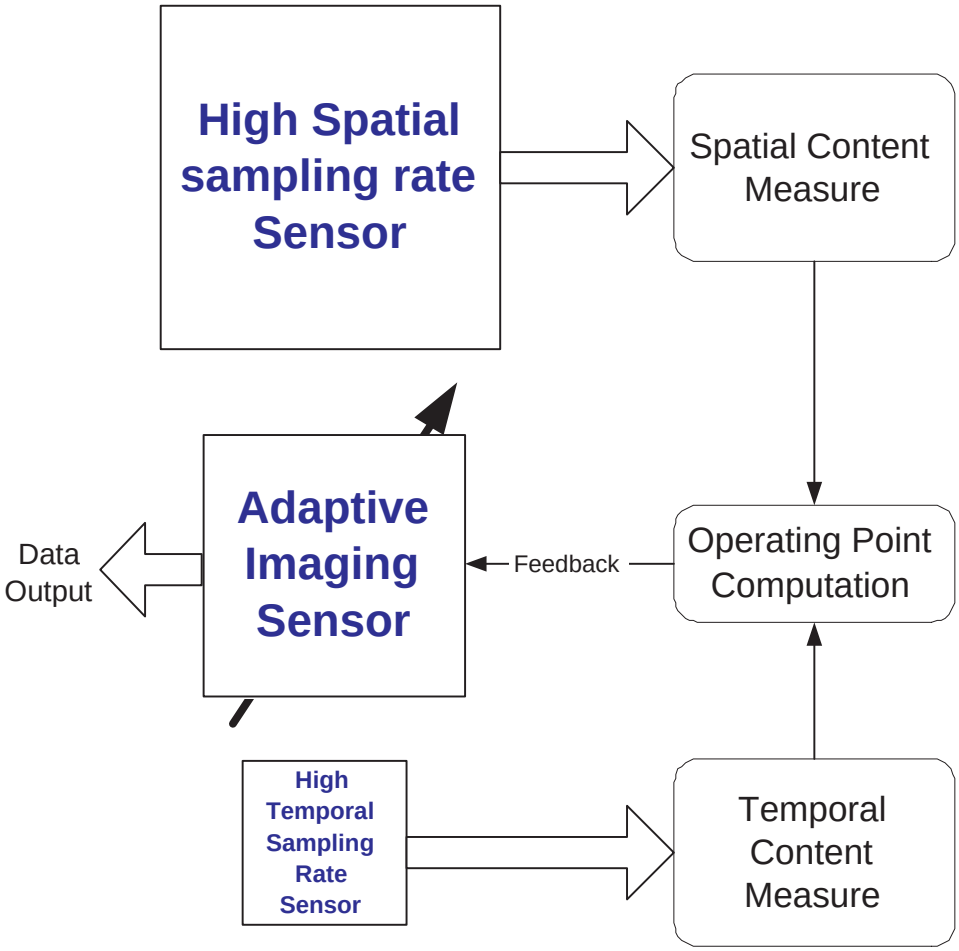

Figure 1.4: An adaptive sensor with three-sensor configuration block diagram

the available bandwidth to increase the spatial sampling rate at the expense of the temporal sampling rate and vice versa.

The video sequence at the output of an adaptive sensor is a set of frames at varying spatial and temporal sampling rates. This three dimensional data cube represents the scene as was sampled by the sensor after adaptation. If the sensor sampled the scene as dictated by the content measure, this cube of data, in the ideal case, should include sufficient information to restore a high resolution spatio-temporal

sequence. In some cases, the sensor operating space will limit the sampling rate and a bias towards the temporal or the spatial sampling rate has to be introduced. In both cases of ideally sampled and under sampled scene, a restoration is possible using methods such as space-time super-resolution [14, 8] and motion compensated interpolation [17].

1.3 Related Work

The use of imaging sensors at different operating points is the basis of other related work. Ben-Ezra and Nayar [2] have used a hybrid sensor configuration to remove motion blur from still images. In their approach, one sensor works in a high temporal, low spatial sampling rate operating point to capture the motion during image integration time. A second sensor acquires the image in high spatial sampling rate and uses the motion information from the first sensor to deblur the image. Lim [12] has employed very high temporal sampling at the expense of spatial sampling to restore a high resolution sequence. Other related work are from the voice recognition field [22, 23]. Here, the use of variable frame rate (VFR) is applied to speech analysis. The frame rate is determined by a content entropy measure on the recorded audio signal.

1.4 Thesis Contribution and Organization

In this thesis we introduce a novel approach for video and image sensing. We have experimentally developed a framework for an adaptive sensor that is simple enough to be implemented as part of the sensor circuit. We explore techniques for measuring the content in a video sequence and the correlation of the content measure to the required sampling rate. The proposed content measure in the framework is robust with respect to noise and aliasing and can be used in a single sensor system configuration. A complete closed loop operation of a single sensor adaptive sensing system has been simulated using natural scene video sequences.

The thesis is organized as follows. In Chapter 2 we explore traditional methods for video content measure and propose a measure based on the ℓ_1-norm operation. We show the advantage of using the proposed measure in terms of behavior with noise and complexity. In Chapter 3 we define the sensor operating point and the way to obtain it from the content measure proposed in Chapter 2. Chapter 4 describes the operation of the sensor as a control system. It describes a real-time open loop experiment and the closed loop simulation along with their results. Chapter 5 conclude the thesis and give insight into future work in this framework.

Chapter 2

Video Content Measure

The purpose of the content measure is to quantify the spatial and temporal information in the scene. By spatial information we mean details or spatial frequency content. Temporal content information is the change along the time axis or temporal frequency content. Accurate measurement of the content will allow us to determine the required sampling rate and to adjust the imaging sensor accordingly. Traditional methods use frequency domain analysis to measure the frequency content of the image sequence. As we show in Section 2.1.1, the frequency domain measure becomes unreliable with the existence of noise. Entropy measures as used in the speech recognition application[23] are computationally inexpensive but seem not to be robust in terms of accuracy for video data content measure. Other methods [21] [15] are based on Shannon's information theory and provide metrics for quality assessment and visualization.

In the adaptive sensor framework,the objective is to keep the computational requirements minimal so that simple and cost effective implementation is possible.

The chosen quantitative measure needs to be robust and accurate in the presence of noise and aliasing. In this chapter we first present the frequency domain and entropy methods for content measure and their characteristics with noise and aliasing. Noting their shortcomings, we then suggest a content measure in the spatial domain that is computationally inexpensive and can work robustly in the present of noise and aliasing. The content measure is first presented for the spatial case. An extension of the suggested measure for the temporal case is described in Section 2.2. In the rest of the thesis we use the proposed spatial and temporal measure in the development of the adaptive imaging framework.

2.1 Spatial Content Measure

The spatial content measure is trying to quantify the spatial information in the scene. By spatial information we mean details or spatial frequency content. In this section we explore the traditional frequency domain and entropy methods, we show their shortcomings and propose a measure based on an ℓ_1-norm operation. An alternative measure based on the ℓ_2-norm operation is briefly described at the end of the section.

2.1.1 Frequency Domain and Entropy Methods

Measuring the spatial content in the frequency domain is naturally translated to a two-dimensional fast Fourier transform (FFT) of the image. The image content is determined to be at the frequency where, say, 99% of the total energy under the spectrum is captured as depicted in Figure 2.1 for a one dimensional signal.

We can define:

$$\mathbf{F} = \mathrm{FFT}_{2D}(\mathbf{X}) \tag{2.1}$$

where $\mathbf{X}$ is a matrix with N pixels presenting the luminance values of the image and $\mathrm{FFT}_{2D}(\cdot)$ is a two dimensional matrix that represents the energy level of the image in the frequency domain. The content measure finds the frequency where most of the total energy in the FFT_{2D} matrix has been captured. Assuming the center of the matrix $\mathbf{F}$ is the DC bin and it has N elements, the content figure is the index such that $\gamma \sum_{i=0}^{N} |\mathbf{F}|_i^2$ has been integrated from the center pixel out. γ is a number close to 1 that determines the point where the frequency energy has significantly dropped.

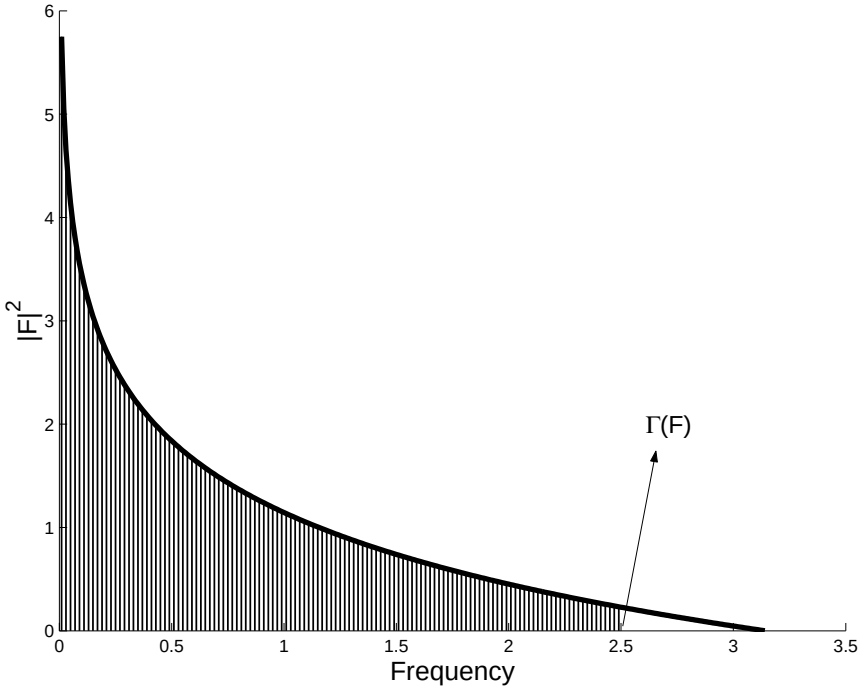

Figure 2.1: $\Gamma(\mathbf{F})$ operator for a one dimensional signal

In the absence of noise, this measure gives an accurate figure for the content

in the image. However, the two-dimensional FFT operation is sensitive to noise. We synthesized a sequence of images for the evaluation of the content measure with respect to spatial bandwidth and noise. The sequence was composed of spatial zoneplate images (Figure 2.2) with frequency content from DC up to a certain known value. The sequence is composed such that the frequency bandwidth of a consecutive zoneplates in the sequence is linearly increasing and all images were sampled above their respective Nyquist rate. Figure 2.2 is an example of four zoneplate images from the simulation with different frequency content.

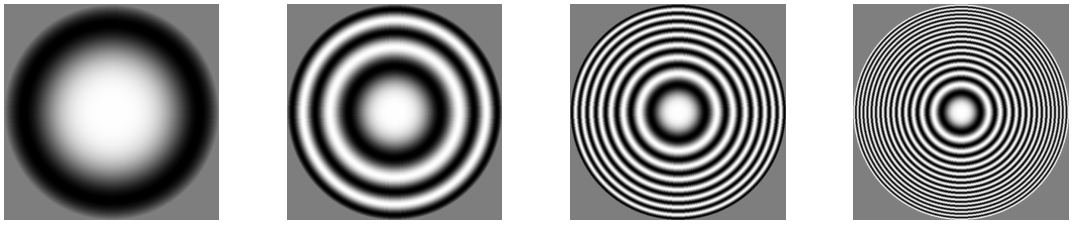

Figure 2.2: Zoneplate images used for the evaluation of the content measure

Figure 2.3 is the simulation results of the frequency domain content measure on the synthesized sequence. The solid line is the content measure of the clean images and it strongly corresponds to the linearly increasing bandwidth of the sequence. The dashed line is the content measure for the same sequence with added white Gaussian noise (WGN) with standard deviation of 20. It is clear that the noise distorts the content measure in a non-linear way such that it does not reflect the image content correctly and makes compensation rather difficult.

Entropy methods for determining signal properties have a wide variety of

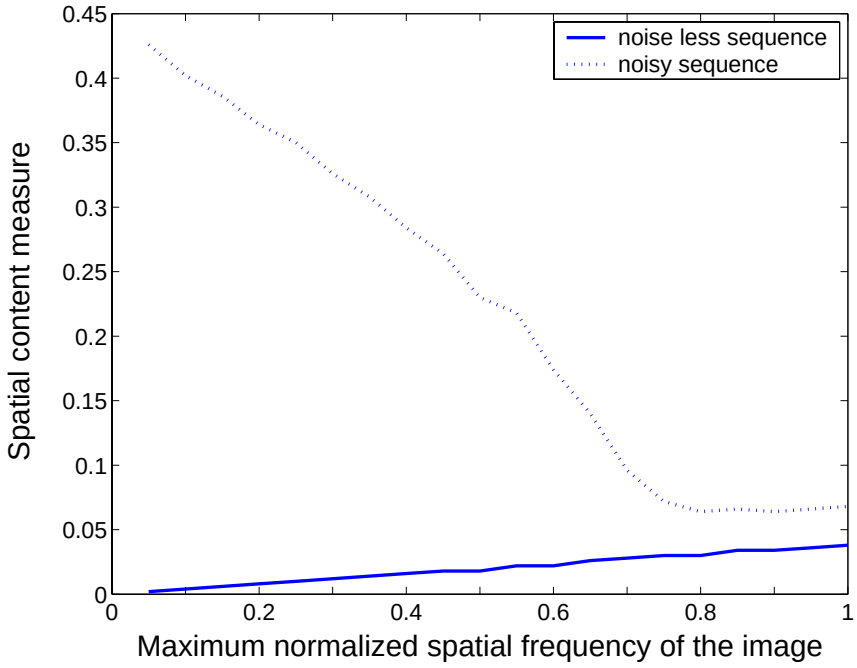

Figure 2.3: Frequency domain spatial content measure

forms. The entropy of a random variable is defined in terms of its probability density and can be shown to be a good measure of randomness or uncertainty. Several authors have used Shannon's entropy [4, 11] and threshold-based entropy to measure the spatial entropy of an image. Shannon's entropy measure is given in Equation 2.2 for an image with N pixels and luminance values x_i, $i = 1..N$.

$$s_{entropy}(\mathbf{X}) \quad = \quad -\sum_{i=0}^{N} x_i log_2(x_i) \tag{2.2}$$

Simulation shows that entropy measure can produce results that are correlated to the image content with higher robustness to noise than then the frequency domain measure. However, the measure is not robust, nor generally useful as it is computed from the entire ensemble of pixels in the considered image without refer-

ence to the relative position of the neighboring gray values. That is, if the pixel gray values at various (or all) positions in a given image are randomly swapped with values at other pixel positions, the very same entropy measure still results. Therefore, it is impossible to relate the scalar output of the measure to the actual content.

2.1.2 Proposed Measure of Content

For a natural image it has been experimentally shown that the differences between adjacent pixel values mostly follow the Laplacian probability density law. Besides we can reasonably assume that in practice these differences are independent from each other [9]. By employing this significant observation, we suggest a methodology to measure the spatial and temporal content. In the proposed framework, obtaining a figure for the content in spatial and temporal domains can be translated to a window operation using ℓ_1-norm as follows. Let $\mathbf{X}$ denote the (say raster scan) vectorized notation of the acquired image with elements $x_{i,j}$. Based on the above statistical model, we first utilize the following nonlinear ℓ_1-based filter [7, 8] applied to each pixel in the image:

$$z_{i,j} = \sum_{m=-p}^{p} \sum_{l=-p}^{p} \alpha^{|m|+|l|} \left| x_{i,j} - x_{i-l,j-m} \right|, \tag{2.3}$$

where the weight $0 < \alpha < 1$ is applied to give a spatially decaying effect to the summation, effectively giving bigger weight to higher frequencies. Other decaying factors can be used such as pixel distance from the center pixel or look-up tables in cases where lower complexity or real-time operation is required. $z_{i,j}$ (or in vector form $\mathbf{Z}$) is directly related to the (log-)likelihood of the image according to the assumed

statistical model. The window operation for $p = 2$ with the decaying factors is illustrated in Figure 2.4. The differences are taken between the center pixel and all the neighboring pixels in the window and weighted by the corresponding decaying factor.

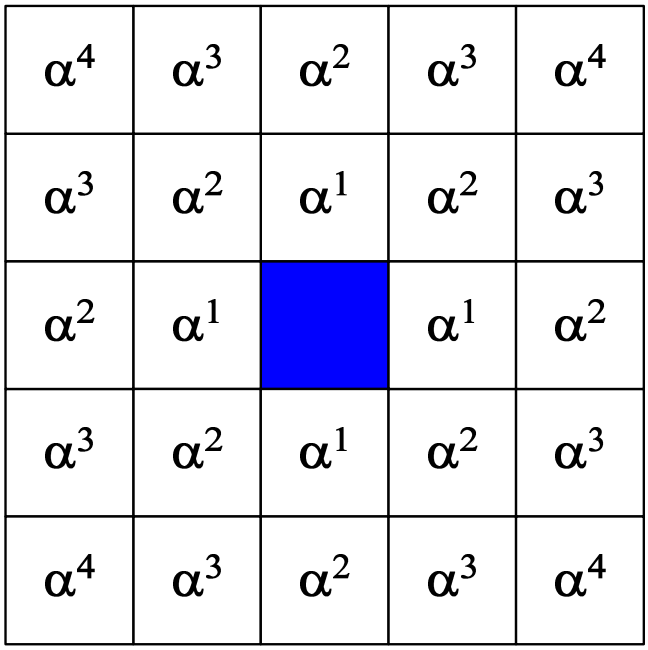

Figure 2.4: The spatial window and the decaying factors of the ℓ_1-norm spatial content measure

To obtain a reasonably robust content measure, one can think of first finding the histogram of $\mathbf{Z}$ (call the value of this histograms $\mathbf{p}_k$ at bin $k = 0, 1, \cdots, M-1$) and then finding the value of the histogram bin (l) such that

$$\sum_{k=0}^{l} \mathbf{p}_k \geq \eta \sum_{k=0}^{M-1} \mathbf{p}_k \tag{2.4}$$

where η denotes the percentage of the total area under the curve we want to contribute in computing the content (for example 95%). Figure 2.5 is an example for a histogram computed on a natural image with $\alpha = 0.5$ and $p = 2$.

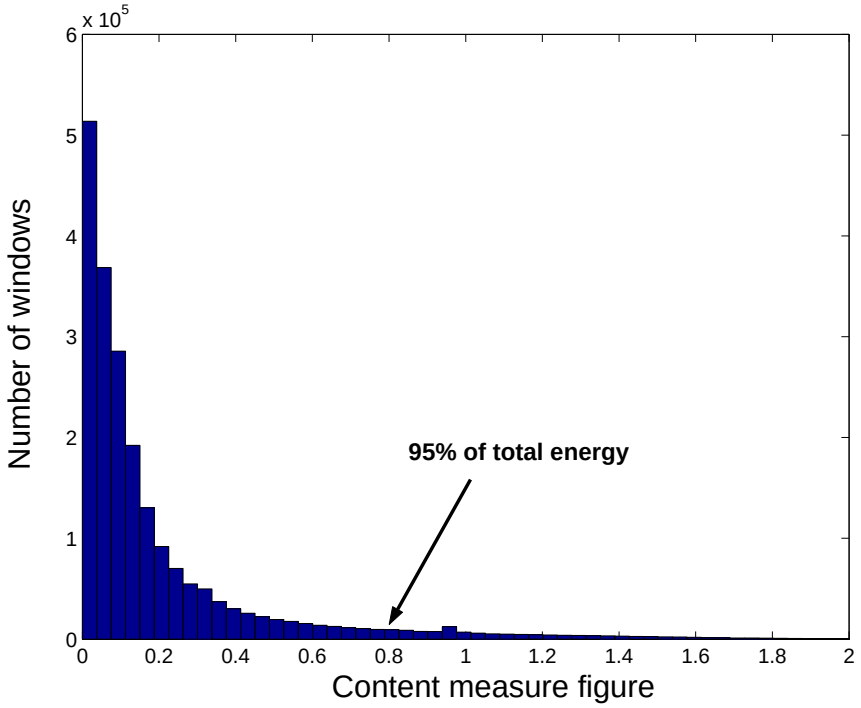

Figure 2.5: Histogram example of the vector $\mathbf{Z}$ for obtaining the content measure

Since computing the histogram in real-time is computationally taxing, a reasonable alternative can be employed based on the Chebyshev inequality[13],

$$p(|\xi - \mu_\xi| \geq c\sigma_\xi) \leq \frac{1}{c^2} \tag{2.5}$$

where μ_ξ and σ_ξ denote the mean and variance of the random variable ξ and $p(\cdot)$ is the probability. From the Chebyshev inequality, we can determine the coefficient c based on the value of η. As an example for $\eta = 0.96$, we have $c = 5$. Next, we compute the mean and variance over the ensemble of elements of $\mathbf{Z}$ ($\mu_{\mathbf{Z}}$ and $\sigma^2_{\mathbf{Z}}$). Finally, the content measure denoted by $\rho(\mathbf{Z})$ is obtained by

$$\rho(\mathbf{Z}) = \mu_{\mathbf{Z}} + c\sigma_{\mathbf{Z}}. \tag{2.6}$$

The proposed ℓ_1-based operation is computationally inexpensive (order of N versus $Nlog(N)$ in the FFT case) and proves to perform well as compared to frequency domain and entropy measures. We characterize the spatial ℓ_1-norm measure with respect to additive white Gaussian noise, measure correlation to the content bandwidth, and analyze its behavior with the presence of aliasing. Figure 2.7 is the simulation results of the ℓ_1-norm content measure on a synthesized sequence with a known frequency content. The sequence is the same one synthesized for the frequency domain measure in Section 2.1.1.

The solid line is the content measure of the synthesized sequence with no added noise. The measure behavior is monotonically increasing and strongly correlates to the linearly increasing bandwidth of the sequence. Figure 2.7 also shows the behavior of the ℓ_1-norm measure for added WGN with different variance (σ^2). As opposed to the frequency domain measure with added noise, the behavior of the ℓ_1-norm measure conserves the ratio of high and low content and can be compensated for rather easily, assuming σ^2 is known [1] or can be estimated [10].

In the simple case where the image data is only white Gaussian noise, the content measure has a pure linear behavior. Figure 2.6 is the simulation result of the ℓ_1-norm spatial content measure for WGN content with varying standard variation. The linear behavior can be explained using the following derivation:

[1] Assuming readout to be the only source of noise, the value of σ^2 can be characterized offline (and hence assumed "known") for a given sensor at a particular operating point.

For a WGN image $\mathbf{X} = \mathbf{W} \sim \mathcal{N}(0, \sigma^2\mathbf{I})$ We get:

$$\begin{aligned} \mu_{\mathbf{Z}} = E(z_{i,j}) &= \sqrt{\frac{4}{\pi}}\sigma \sum_{m=-p}^{p} \sum_{l=-p}^{p} \alpha^{|m|+|l|} \\ &= \sqrt{\frac{4}{\pi}}\sigma \left[\left(2\frac{1-\alpha^{(p+1)}}{1-\alpha} \right)^2 - 1 \right] \end{aligned} \tag{2.7}$$

$$\begin{aligned} \sigma^2_{\mathbf{Z}} = VAR(z_{i,j}) &= 2\sigma^2 \sum_{m=-p}^{p} \sum_{l=-p}^{p} \alpha^{2|m|+2|l|} \\ &= 2\sigma^2 \left[\left(2\frac{1-\alpha^{(2p+2)}}{1-\alpha^2} \right)^2 - 1 \right] \end{aligned} \tag{2.8}$$

Referring to Equation 2.6 we can see that in the case of WGN only the content measure is linear with the noise standard deviation (σ).

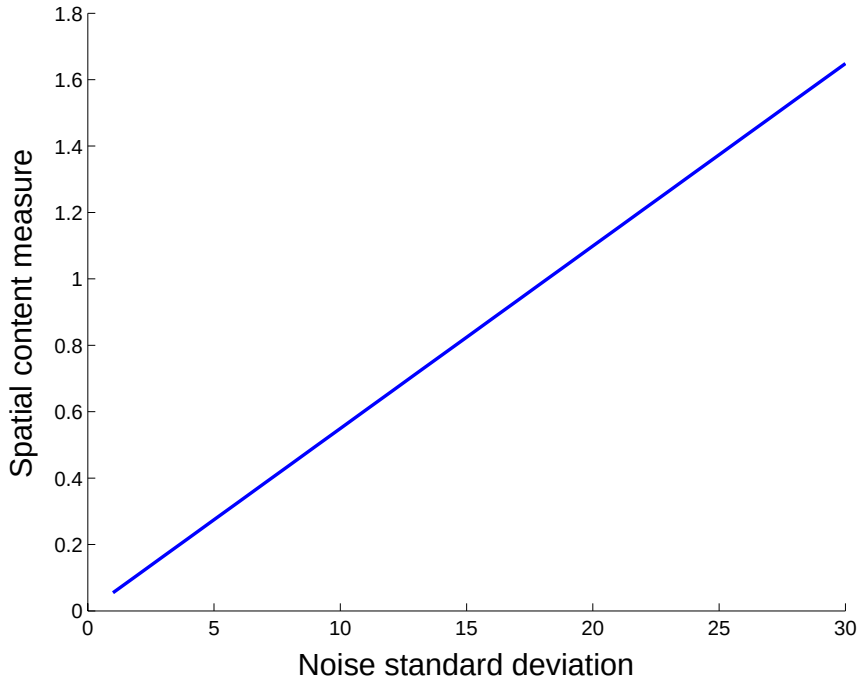

Figure 2.6: ℓ_1-norm spatial content measure behavior for WGN content

In natural scenes, the $x_{i,j}$ in Equation 2.10 are not independent values. Since the ℓ_1-norm is not a linear operation, a simple analytical derivation for the behavior of the measure is rather difficult to find. As shown in Figure 2.7, additive noise creates a non-linear behavior to the content measure that can be modelled and compensated for.

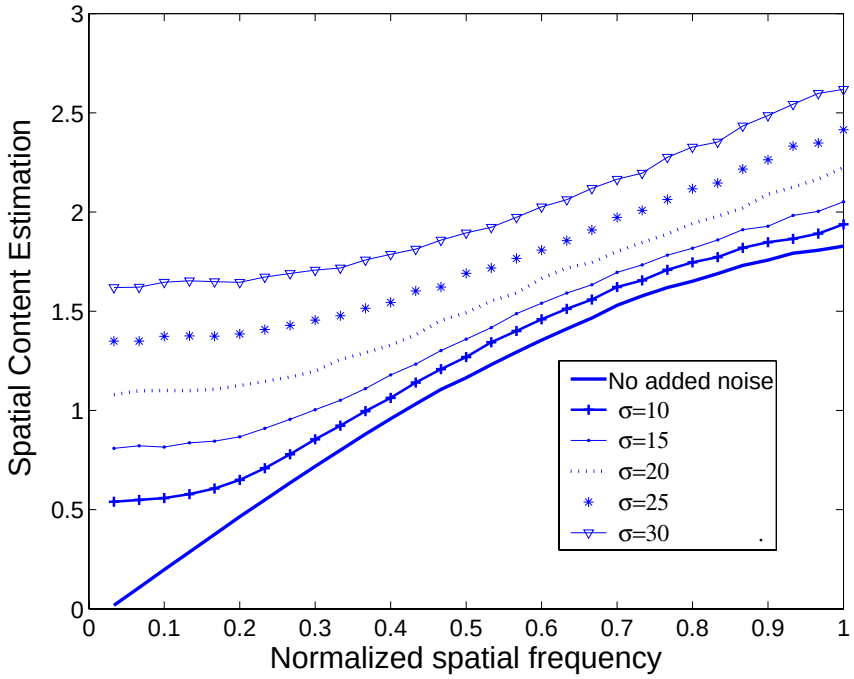

Figure 2.7: ℓ_1-norm spatial content measure with added WGN

Using large data base of training data, the compensation is done by characterizing the bias between the noisy measure and the pure measure for the range of possible noise levels. This characterization leads to a 4^{th} order polynomial that provide the bias level with respect to the noise standard deviation (σ). The general behavior as shown in Figure 2.7 is that content that produce low content measure will

suffer from larger bias and the bias is approximately constant as the content figure exceed a certain level. Figure 2.8 provides the bias behavior along with its polynomial fit for noisy measures with $\sigma = 10$, $\sigma = 20$, and $\sigma = 30$. Equation 2.9 is an example for a polynomial fit of the noise bias with respect to the content measure (ρ) for $\sigma = 20$. The polynomial coefficients can be tabulated with respect to σ for different noise levels.

$$\begin{aligned} &\textit{Content Measurement Bias}_{(\sigma=20)} \quad = \\ &\qquad 3 * 10^{-9}\rho^4 - 2.8 * 10^{-6}\rho^3 \quad + \quad 0.00059\rho^2 - 0.041\rho + 1.1 \end{aligned} \tag{2.9}$$

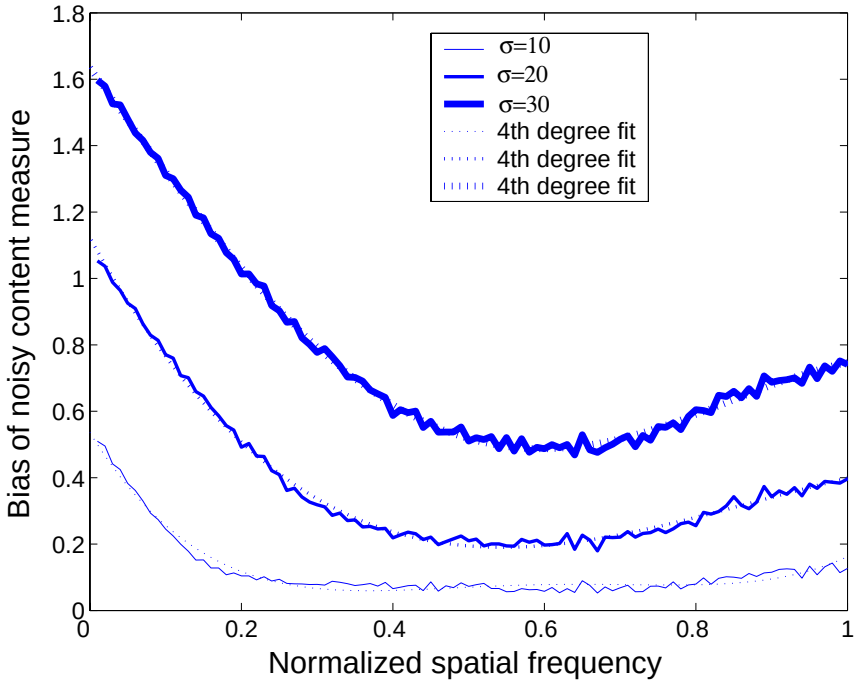

Figure 2.8: Noisy measure bias and corresponding polynomial fits for different noise levels

Experiments with natural video show that this compensation method can remove the bias such that the compensated measure is consistently within 10% of the

noise-less measure. Figure 2.9 is a simulation of a spatial content measure of a natural video sequence with added noise of $\sigma = 20$. The figure shows the pure measure along with the noisy and the compensated measures.

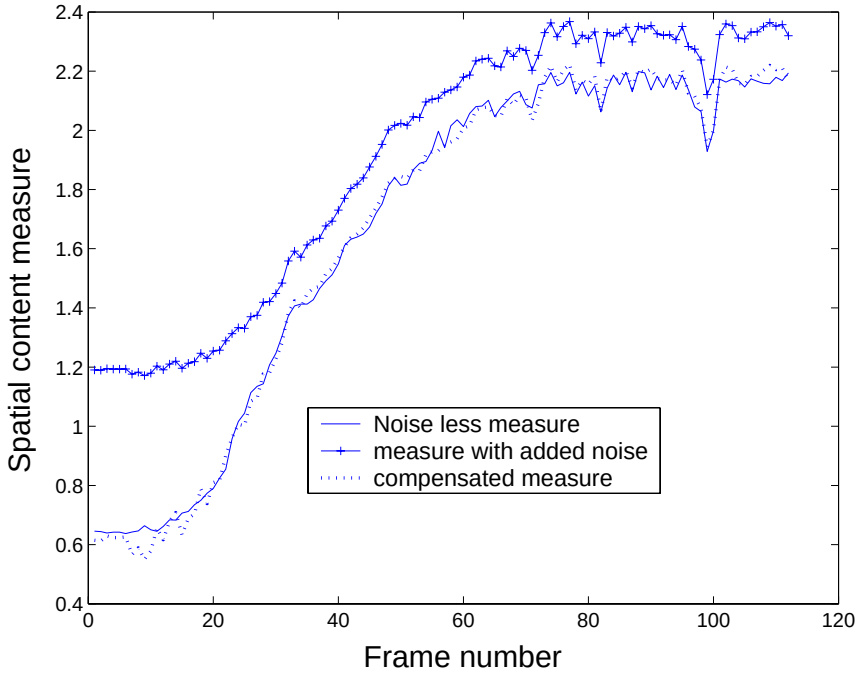

Figure 2.9: Example of noise compensation in a natural video sequence with $\sigma = 20$

As further discussed in Chapter 3, aliasing effect in the ℓ_1-norm measure was evaluated by down-sampling the synthesized sequence to introduce aliasing. Simulation results show that the measure saturates as soon as aliasing is introduced so that high to low content ratio is still kept. This is an important characteristic for a content measure since the adaptive sensor may run at any point in time in an operating point that introduces aliasing.

2.1.3 Spatial content measure using ℓ_2-norm

An alternative measure to the proposed ℓ_1-norm is a similar measure that uses the ℓ_2-norm operation. The content measure in the spatial domain can be translated to a window operation using ℓ_2-norm as follows:

$$y_{i,j} = \sum_{m=-p}^{p} \sum_{l=-p}^{p} \alpha^{|m|+|l|} \left(x_{i,j} - x_{i-l,j-m}\right)^2, \tag{2.10}$$

The content figure is obtained from the matrix $\mathbf{Y}$ using Equation 2.6. In the simple case where the image data is only white Gaussian noise, the content measure has a pure linear behavior with σ^2.

$$\begin{aligned} \mu_{\mathbf{y}} = E(y_{i,j}) &= 2\sigma^2 \sum_{m=-p}^{p} \sum_{l=-p}^{p} \alpha^{|m|+|l|} \\ &= 2\sigma^2 \left[\left(2\frac{1-\alpha^{(p+1)}}{1-\alpha} \right)^2 - 1 \right] \end{aligned} \tag{2.11}$$

$$\begin{aligned} \sigma^2_{\mathbf{y}} = VAR(y_{i,j}) &= 12\sigma^4 \sum_{m=-p}^{p} \sum_{l=-p}^{p} \alpha^{2|m|+2|l|} \\ &= 12\sigma^4 \left[\left(2\frac{1-\alpha^{(2p+2)}}{1-\alpha^2} \right)^2 - 1 \right] \end{aligned} \tag{2.12}$$

Figure 2.6 is the simulation result of the ℓ_2-norm spatial content measure for WGN content with varying standard variation.

Figure 2.11 shows the behavior of the ℓ_2-norm measure with linearly increasing content as well as with added noise in different levels. The behavior of the ℓ_2-norm measure is very similar to the ℓ_1-norm in terms of correlation of the measure to the

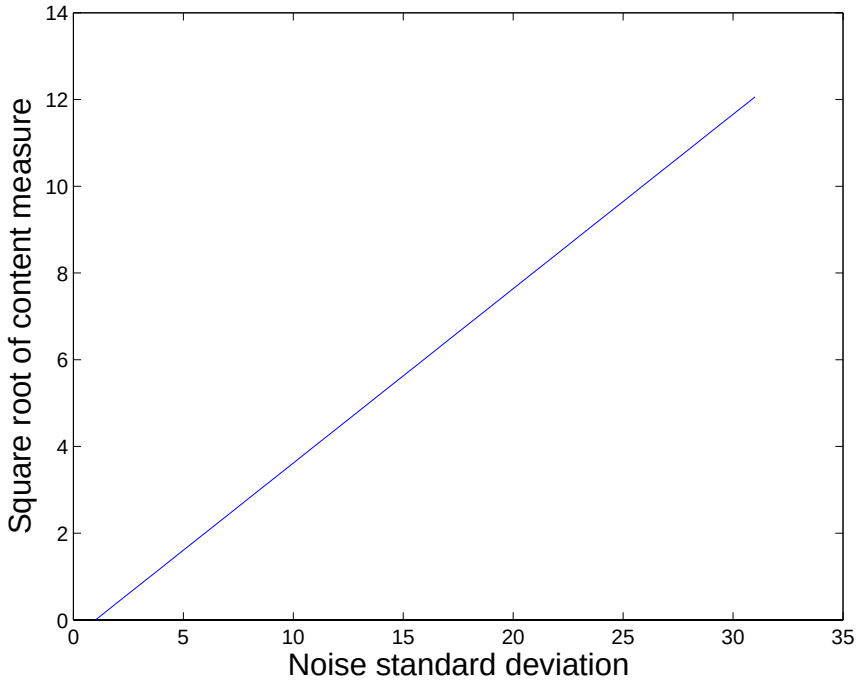

Figure 2.10: ℓ_2-norm spatial content measure behavior for WGN content

content. However, the noise effect on the measure is mainly bias which makes the noise compensation easier.

Although the ℓ_2-norm operation provides good measure of content and it is robust with noise, it does not have a direct correlation to the statistical model of the differences between adjacent pixel values as the ℓ_1-norm provides. Moreover, it is computationally more expensive due to the power operation.

2.2 Temporal content measure

Measuring of the temporal content in a video sequence is the companion problem to the spatial content measure in an image. Here we quantify the temporal information in the scene. The same ℓ_1-norm method as in the spatial case can be used

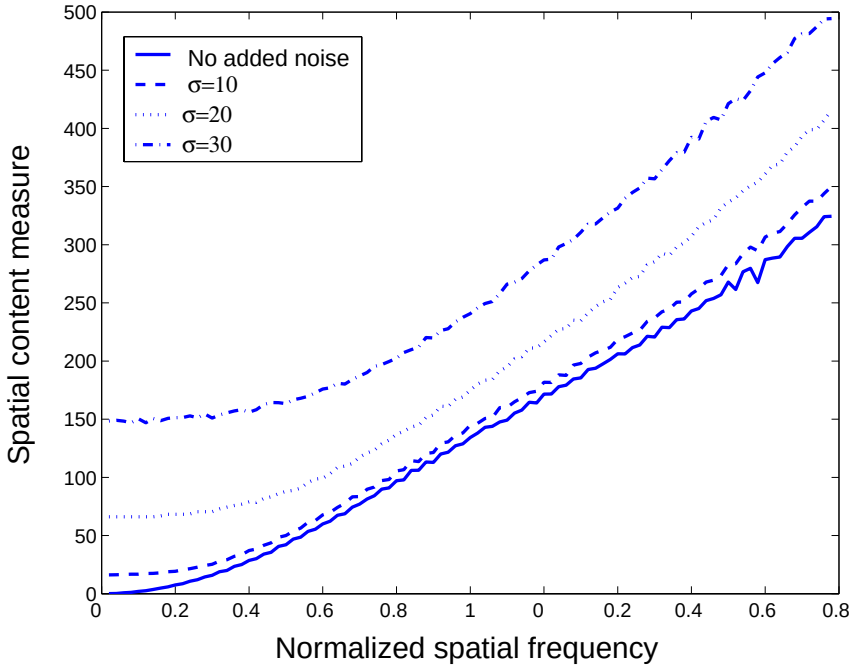

Figure 2.11: ℓ_2-norm spatial content measure with added WGN

on a one dimensional window along the time axis in the following form:

$$q_{i,j,t} = \sum_{k=-p}^{p} \beta^{|k|} \left| x_{i,j,t} - x_{i,j,t+k} \right| \tag{2.13}$$

where the operation is performed on a window of duration $2p+1$ time samples and the scalar weight $0 < \beta < 1$ is applied to give a temporally decaying effect to the summation, effectively giving bigger weight to higher temporal frequencies. The window operation for $p = 2$ with the decaying factors is illustrated in Figure 2.12. The differences are taken between the center pixel and the neighboring pixels in the window and weighted by the corresponding decaying factor. An alternative operation to the ℓ_1-norm in Equation 2.13 is the ℓ_2-norm operation as described in Section 2.1.3.

The content figure is given by $\rho(\mathbf{Q}_t)$ where $\mathbf{Q}_t$ is the matrix notation for $q_{i,j,t}$

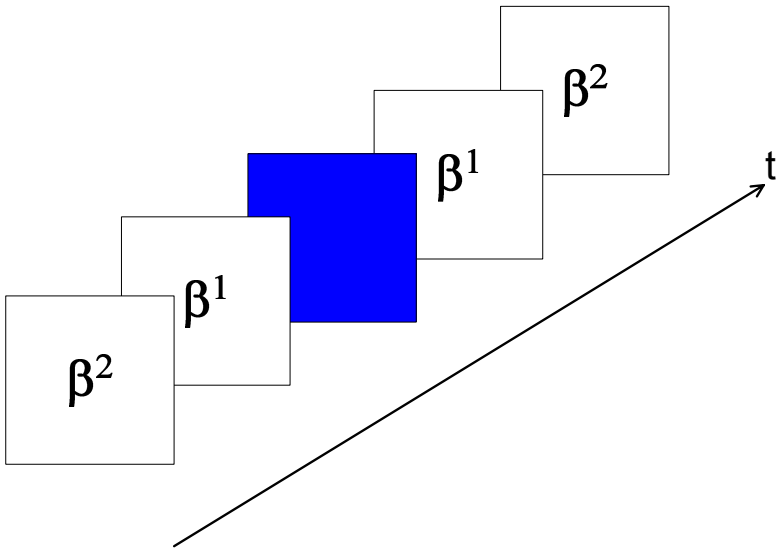

Figure 2.12: The temporal window and the decaying factors of the ℓ_1-norm temporal content measure

(at frame t) and the same $\rho(\cdot)$ operator as defined in Equation 2.6 is used to compute the temporal content measure. The ℓ_1-norm operation on the one dimensional window provides the same linear behavior with noise only sequence as given in Equations 2.14 and 2.15 and shown in Figure 2.13.

$$\begin{aligned} \mu_{\mathbf{q}} = E(q_{i,j,t}) &= \sqrt{\frac{4}{\pi}}\sigma \sum_{k=-p}^{p} \beta^{|k|} \\ &= \sqrt{\frac{4}{\pi}}\sigma \left[2\frac{1-\beta^{(p+1)}}{1-\beta} - 1 \right] \end{aligned} \tag{2.14}$$

$$\begin{aligned} \sigma^2_{\mathbf{q}} = VAR(q_{i,j,t}) &= 2\sigma^2 \sum_{k=-p}^{p} \beta^{2|k|} \\ &= 2\sigma^2 \left[2\frac{1-\beta^{(2p+2)}}{1-\beta^2} - 1 \right] \end{aligned} \tag{2.15}$$

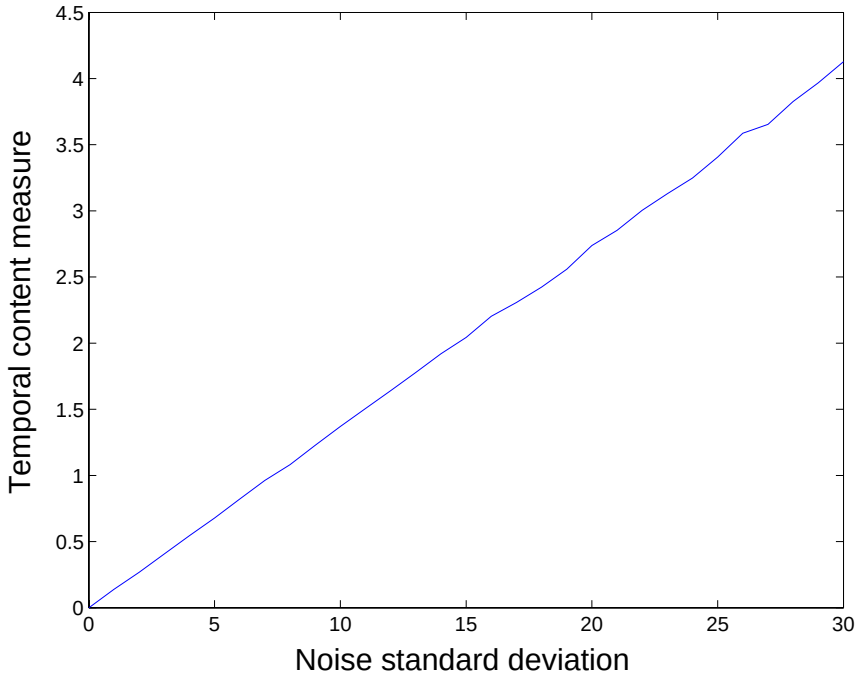

Figure 2.13: ℓ_1-norm temporal content measure behavior for WGN content

Figure 2.14 is the simulation results of the temporal ℓ_1-norm content measure on synthesized sequences. It also shows the behavior of the measure to added WGN with different variance levels. The synthesized sequences were composed with a known temporal frequency content by changing the pixels value along the time axis using a sinusoid. Figure 2.15 is an example of pixels value along the time axis from four different sequences. Each sequence has different temporal content according to the sinusoid being used. The measure characteristics with respect to additive noise, correlation to the content bandwidth, and behavior with the existence of aliasing, are similar to its counterpart in the spatial domain.

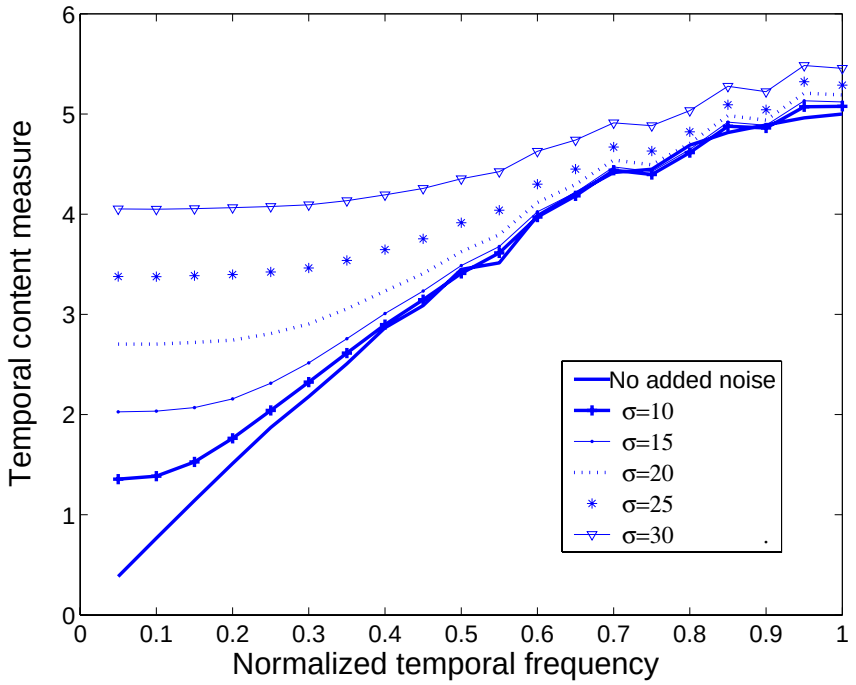

Figure 2.14: ℓ_1-norm temporal content measure with added WGN

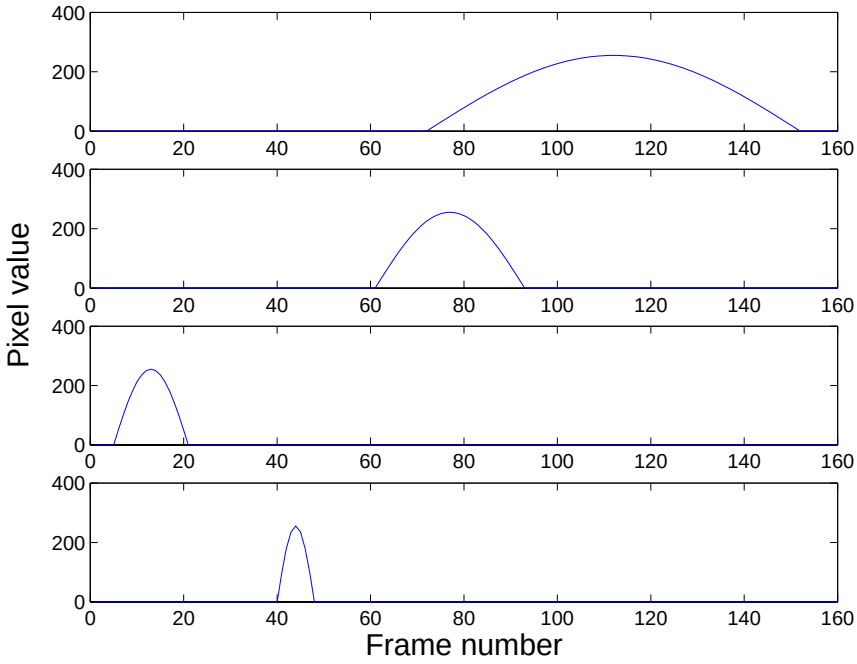

Figure 2.15: Pixels value along the time axis of synthesized sequences for the evaluation of the temporal content measure

Chapter 3

Sensor operating point

In Chapter 2 we explored the means to measure the spatial and temporal content in the scene using the data retrieved from the sensor. Although not directly, the content measure dictates the required sampling rate of the scene. The required sampling rate is used to adjust the temporal and spatial operation of the sensor according to its capabilities. In this chapter we define the operating point and operating space of the sensor. We give the means to convert the ℓ_1-norm content measure to the required operating point and describe the projection operation of that point to the sensor operating space.

3.1 Operating point definition

The sensor operating point (SOP) is defined as {number of pixels per frame, frame rate} point in the feasible space of the sensor as depicted, for example, in Figure 3.1. The sensor's operating space is different from sensor to sensor and may not be smooth due to physical limitations such as circuit timing and limited interpolation capabilities that are required for non-integer spatial sampling rates. The

temporal sampling rate is more flexible since it is directly controlled by the logic circuit of the sensor. Spatially, the sensor is arranged into pre-defined array of pixels and sampling rate can be changed in a discrete manner using decimation or binning techniques. Changing the spatial sampling rate continuously requires interpolation or special physical design of the pixel array.

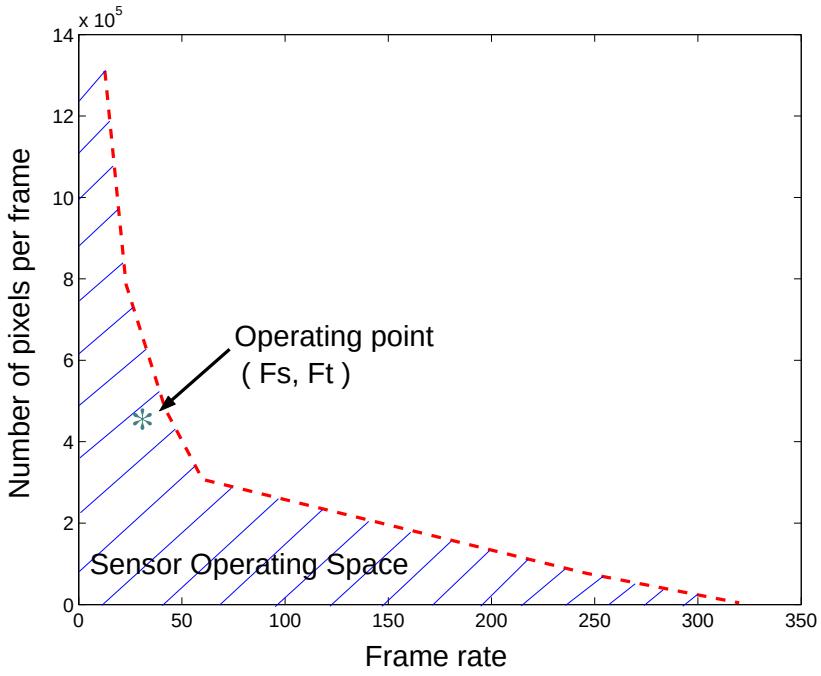

Figure 3.1: Example of sensor operating space and operating point

The required operating point (ROP) is defined as the {number of pixels per frame, frame rate} set as dictated by the scene. In other words, the ROP is the minimum required temporal and spatial sampling rates that avoid aliasing or allow for full restoration of the video sequence by post-processing. In this framework we would adjust the SOP to be as close as possible to the ROP, adapting the imaging process to the sensor's capabilities and the scene.

3.2 Operating point computation

The ROP is derived from the spatial and temporal content measures. Ideally, the spatial content measure would be computed by a spatially high resolution sensor to obtain an accurate non-aliased measure. Similarly, the temporal content would be ideally measured by a high frame rate sensor such that the temporal information in the scene is measured accurately. The actual imaging would be done by a third sensor that is running at varying operating points. A block diagram for such a sensor is depicted in Figure 1.4. The three-sensor configuration may be too expensive in practical applications and requires relatively complicated optics. In practice we would like to measure the content in the scene using the same sensor that is used for imaging. This may reduce the accuracy of the content measure due to possible aliasing. Using the ℓ_1-norm content measure, the single sensor accuracy problem will only effect the operating point transitions when significant content changes occur in the scene. The system will always converge to the correct operating point as further discussed in this section and in Chapter 4.

The spatial and temporal content measures produce two scalar figures for each frame of the video sequence. The content measure is the output of the ℓ_1-norm operation and does not have a direct relation to the required sampling rate. The conversion from content measure to ROP is done through the use of synthesized video sequences with known spatial and temporal bandwidth. Taking these sequences through the content measure operations we create spatial and temporal conversion

curves.

We show an example of the operating point computation where we take synthesized video and compute the content measures from it. For the spatial conversion, the sequence is composed of zoneplate images as described in Section 2.1.1 but with single frequency content for maximum accuracy. The temporal operating point computation is done through a similar concept in the time axis. The synthesized sequences for the temporal case are described in Section 2.2 and shown as example in Figure 2.15.

Since the characteristics of the conversion are different from one operating point to another, we use a separate conversion curve for each operating point. Figure 3.2 shows the spatial content measure to required sampling rate conversion curves. Figure 3.3 shows the conversion curves for the temporal case. The curves that are presented in those figures are for pre-defined discrete operating points. The simulation for creating the curves uses a high sampling rate non-aliased sequence as the baseline and creates lower sampling rate sequences by down sampling. The down-sampled sequences introduce aliasing as expected.

As shown in Figure 3.2, the spatial content measure for an aliased image will saturate the ℓ_1-norm operator, indicating that the current sampling rate is insufficient. This characteristic is essential for the closed loop operation of the adaptive sensor as described in Chapter 4. The temporal conversion in Figure 3.3 has the same saturation characteristic with additional bias effect. The bias effect is caused by the motion scaling that takes place in the temporal down sampling action (motion will be larger between two consecutive frames of the down sampled sequence as compared to the

original sequence). If an imaging sensor supports continuous operating points within its operating space, then Figures 3.2 and 3.3 are the actual conversion to the required sampling rate. If the sensor supports only discrete points within its operating space, we can create a look-up table for the conversion by setting thresholds in the conversion curves at these discrete points.

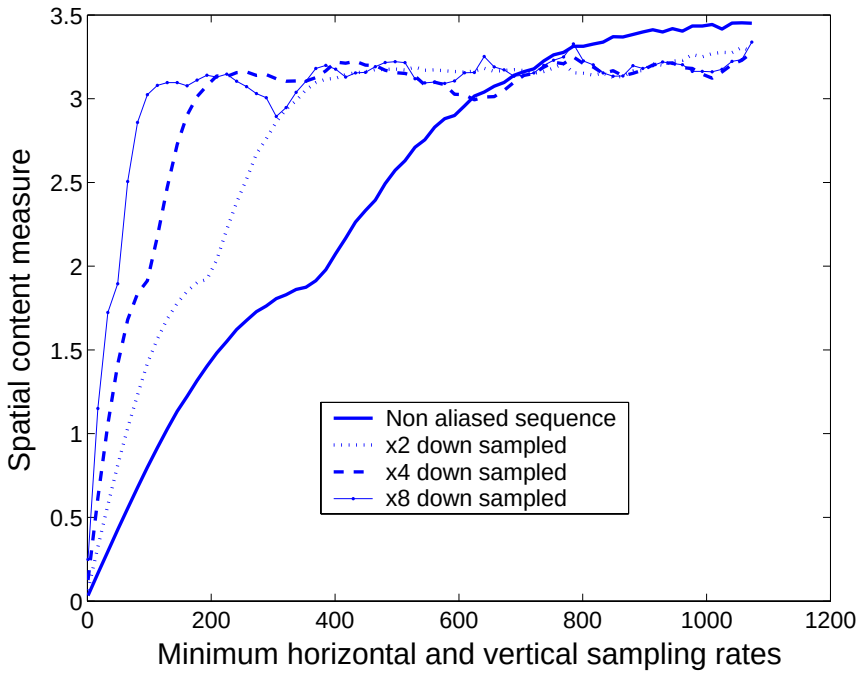

Figure 3.2: Spatial content measure to sampling rate conversion

3.3 Projection to the sensor operating space

The required operating point reflects the minimum required sampling rate as dictated by the scene. In some cases this point falls within the sensor operating space, but in other cases the ROP may fall outside. These two cases are depicted in Figures 3.4 and 3.5 respectively. In the closed loop operation we need to determine the new

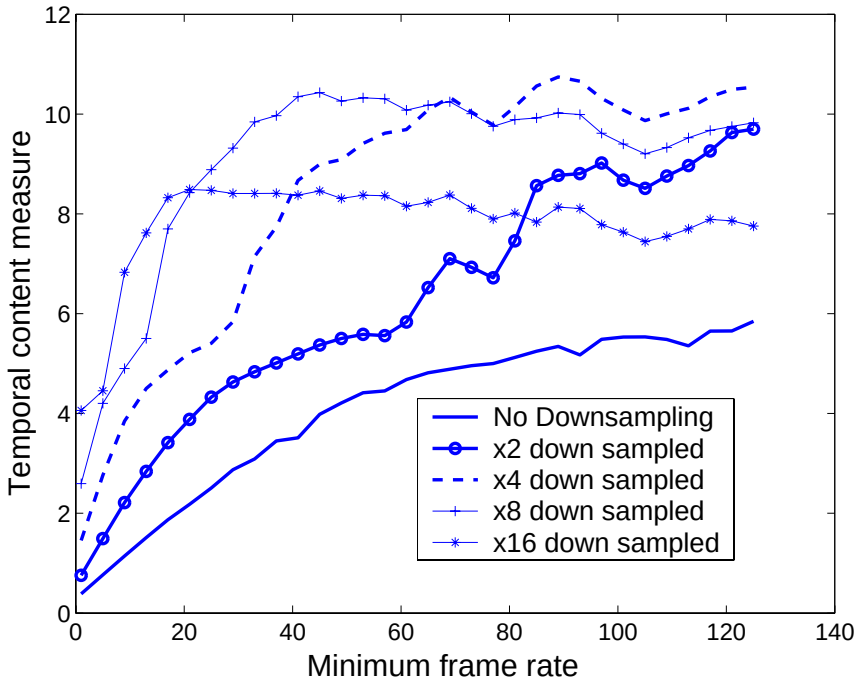

Figure 3.3: Temporal content measure to sampling rate conversion

sensor operating point (SOP) for every frame.

In the case where the operating point falls inside the sensor operating space, there are two options for determining the new sensor operating point. If the objective is to minimize the bandwidth at the output of the sensor then ROP=SOP. That is because the ROP is computed from the content measure that obtains the minimum required sampling rate. In the case where the data bandwidth is second in priority, the SOP can be shifted (if possible) to higher sampling rates above the minimum defined by the ROP. The shift can be done in the temporal, spatial or both axes depending on the available bandwidth and user preferences. This shift is depicted by the dashed arrows in Figure 3.4. Here we refer to user preferences as the option to shift the

operating point towards higher temporal or spatial sampling rate when the option exists. That allows the user to create a sequence that has higher temporal or spatial quality respectively.

In the case where the operating point falls outside the sensor operating space, the sensor does not have sufficient bandwidth to capture the scene and additional projection operation is required. The most natural projection is to the closest possible operating point in the sensor operating space as depicted in Figure 3.5. Here again the user can bias the projection toward higher spatial or temporal sampling rate. However, in this case the bias will improve the sampling rate of one domain at the expense of the other.

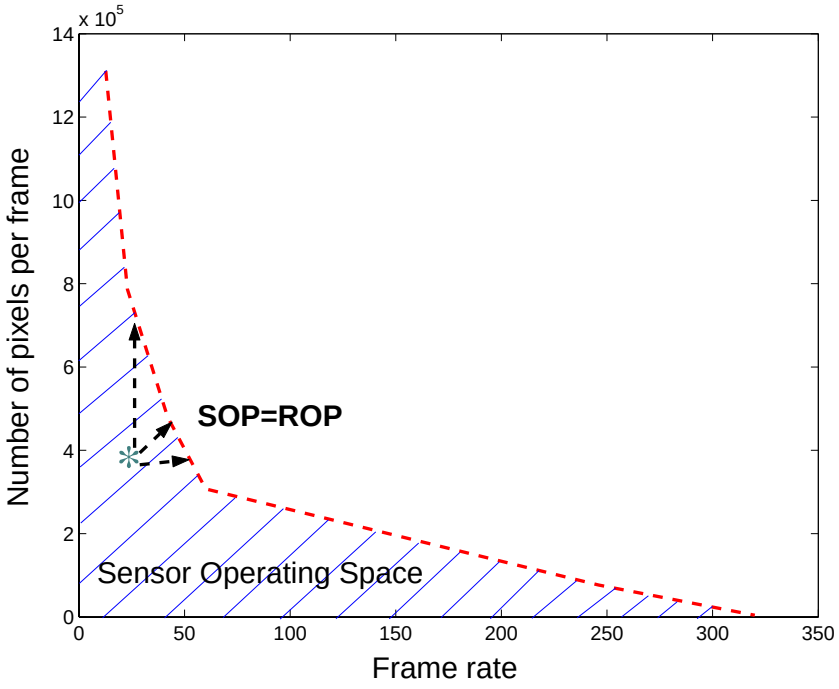

Figure 3.4: Projection of operating point to sensor operating space - point is within the space

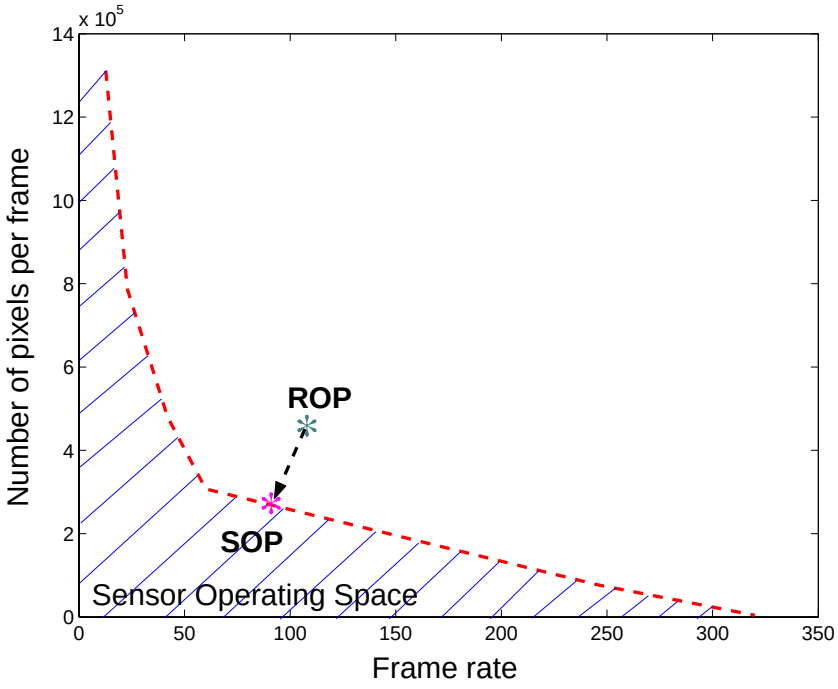

Figure 3.5: Projection of operating point to sensor operating space - point is outside the space

Chapter 4

Closed loop operation

In previous chapters we introduced the content measures and the sensor operating point and gave the way to obtain them from the sensor data. In this chapter we describe the closed loop operation of an adaptive sensor. Adaptive imaging can be described as a control system as it has a proper feedback loop that adjust the system to track the scene. A real-time experiment in open loop was conducted for the evaluation of the content measures and possible approaches for the operating point feedback operation. The experiment is presented in Section 4.2. A complete closed loop simulation of an adaptive imaging sensor was created and the results are presented in Section 4.3.

4.1 Adaptive imaging control system

Adaptive imaging can be depicted as a control system that tracks the scene through measuring its content. As illustrated in Figure 4.1, the sensor's output is the system output as well as the feedback loop mechanism's input. The information about the scene is extracted in the first step of the feedback loop by the content

measure block. The content measure is converted to the required operating point using conversions curves or look-up tables that were prepared according to the imaging sensor capabilities as described in Section 3.2. The computed operating point may or may not be within the sensor's operating space. Therefore, an additional stage of projecting the required operating point to the sensor operating space is required. The projection operation is described in details in Section 3.3.

Finally the error in the system between the current operating point and the computed one is determined and fed back to the sensor through a feedback filter. The filter in the feedback loop is effectively smoothing the feedback response and keeps the system from diverging. In a sensor with discrete operating point, the filter can be as simple as restricting the change in the operating point to the nearest one in any direction. For a continuous operating space sensor the filter can perform a smoothing operation as follows,

$$\mathrm{SOP}(t) = \mathrm{SOP}(t-1) + \Delta\mathrm{SOP}_c(t) \tag{4.1}$$

where SOP_c is the SOP that was calculated at time t and Δ operates as a gain, controlling the amount of smoothing on the operating point behavior. The sensor operation normally starts in a middle range operating point and converges within few frames. The rate of convergence depends directly on the feedback filter gain.

As described in Chapter 3, the ROP to sampling rate conversion will saturate whenever the content is aliased for the current operating point. This important characteristic of the conversion will ensure the convergence of the system since the

saturated value will drive the sensor to a higher sampling rate until no aliasing occur and the content measure is accurate again or until the sensor has reached its limits.

The convergence speed mainly depends on the feedback loop gain and filter design. The optimal evaluation will be with a sensor that has continuous operating space. In the closed loop simulation we use discrete operating points due to limitation in the process of creating the sensor operating space. In this case the filter simply restricts the operating point to do one step at the time spatially or temporally. Therefore, the convergence is guaranteed to be within δ frames, where δ is the discrete distance between the current and the new operating point.

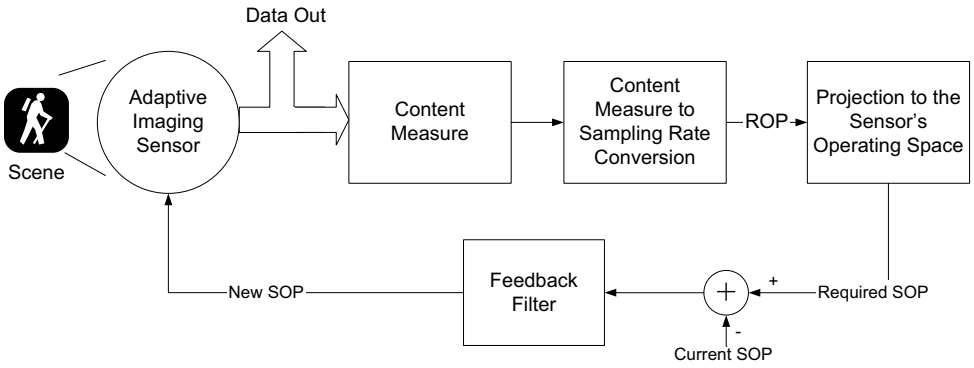

Figure 4.1: Closed loop operation

4.2 Real-time open loop experiment

The adaptive sensor relies on real-time data processing for the capture of the scene content. In order to evaluate the robustness of the content measures as well as the SOP computation, a real time setup was developed. The setup includes a

IEEE1394 camera and a PC. The Windows drivers for the camera were obtained from the robotics institute at Carnegie Mellon university [6].

The purpose of this driver set is to provide easy, direct access to the controls and imagery of compliant cameras on the IEEE1394 serial bus [1]. These cameras are capable of transmitting image data at up to 400 mbps while also offering the ability to control myriad parameters of the camera from software. Having the drivers and application source code available, the frames from the camera are captured by relatively minor chances in the software. Additional control can be added to the user interface for parameter changing in real-time manner. Since the data from the sensor is captured with no compression, the data can be processed with no additional artifacts and displayed in real-time. The real-time processing capability depends on the particular PC performance being used and the complexity of the processing software. This setup provides a powerful tool for development and testing of image processing algorithms.

In this experiment we used a Pyro webcam from ADS technologies [20] which seamlessly connects to the CMU drivers and provides a wide variety of video resolutions and control. The spatial and temporal content measures were implemented to work in real-time and give a graphical display of the results. The camera was running at a constant rate of 320×240 spatially and 30 frames per second temporally. The user interface is providing control over the measure parameters such as the decaying factors α and β and the window size of the content measures. Screen capture of the Windows environment is shown in Figure 4.2. The specific control panel that was created for

this experiment is shown in Figure 4.3.

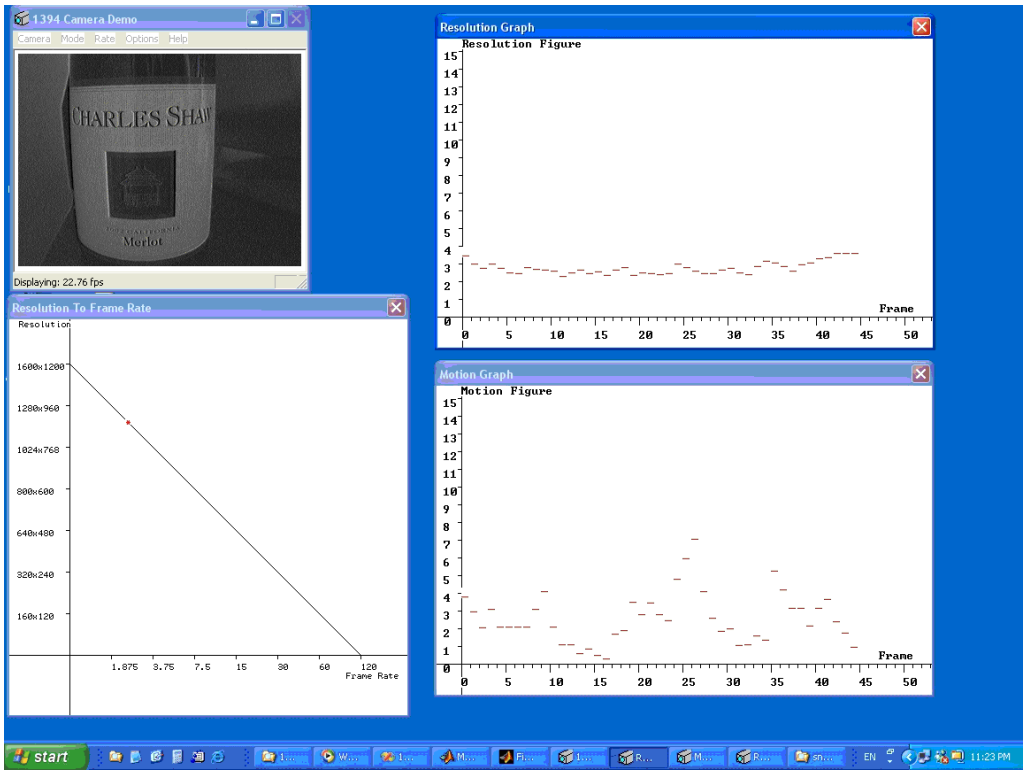

Figure 4.2: Video and graphic display of the IEEE1394 real-time experiment

The real-time graphic display and control proved the robustness of the content measures throughout various scenes and conditions. Both the temporal and spatial measures were tested with natural indoors and outdoors scenes to check the correlation of the measure to the content and behavior with noise. A simple conversion from the content measure to sensor operating point was manually created using look-up table of 10×10 entries. The new operating point is graphically displayed for the evaluation of possible approaches towards the development of the content measure to sampling rate conversion as being used in the closed loop operation. This experiment mainly provides

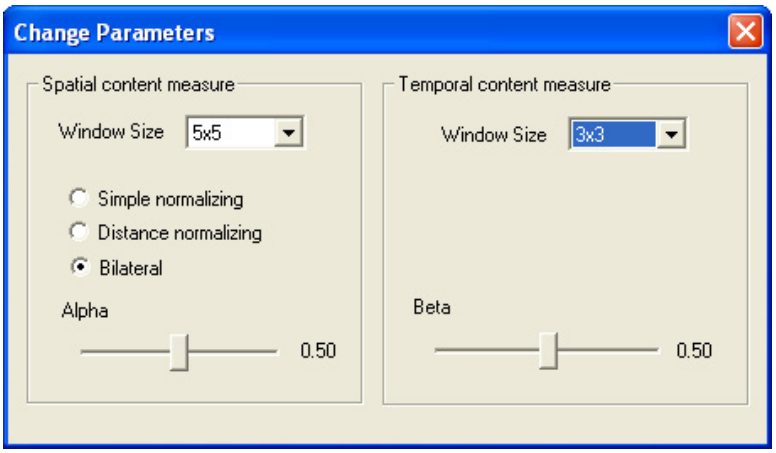

Figure 4.3: Content measure control window of the IEEE1394 real-time experiment

a setup for varying the different parameters in different conditions and observing the behavior of the content measure and operating point.

Using a more sophisticated camera such as PL-A742 of PixeLink [19] or MotionXtra HG-SE of Redlake [3], this real-time open loop experiment can be extended to work in closed loop and provide an adaptive imaging system that can be controlled by a user through the PC. The data can be stored for post processing or can be post processed at real-time if computation permits.

4.3 Closed loop simulation

The complete closed loop system was simulated using real sequences from a high definition television video source. The high definition video is composed of 1920×1088 images at 60 frames per second frame rate. By down-sampling this sequence spatially and temporally, we created several discrete operating points as depicted in Figure 4.4. Since the original sequence is sampled at high sampling rate

spatially and temporally, the down sampling operation could be done using integer values only and avoiding any interpolation that could warp the data. The operating space of this simulated sensor is large enough to demonstrate the transitions in operating points and system convergence.

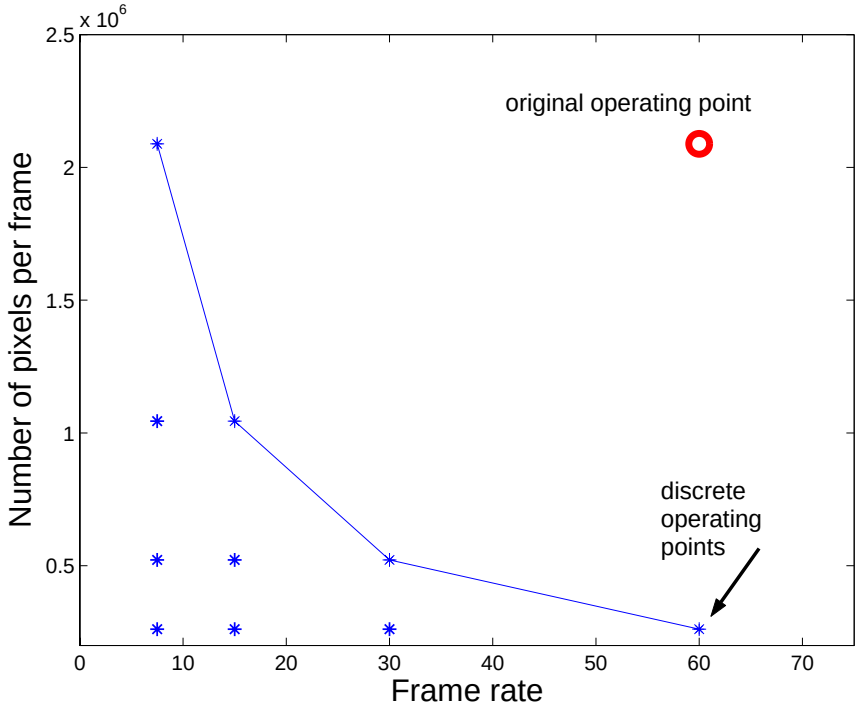

Figure 4.4: Operating space created for the closed loop simulation

The conversion from ROP to sampling rate has been tabulated using thresholds as described in Chapter 3. For the spatial conversion we use the curve in Figure 3.2 and set the thresholds at the discrete operating points available for the simulation. Similarly, the temporal conversion is using the curve from Figure 3.3. The system output was evaluated through a simple display mechanism where images were spatially scaled and temporally repeated to create a high spatio-temporal sampling

rate sequence. The simulation output results in a new sequence that has significantly reduced data bandwidth at certain points. The bandwidth reduction can be as significant as 40% of the original sequence for static scenes or scenes with low spatial bandwidth. The operating point dynamics show high correspondence to the image bandwidth as measured in the frequency domain.

Figures 4.5(a) and (b) are the spatial and temporal content measures along 900 frames of a high definition video sequence. We marked the major operating point transitions along the curves and show the corresponding images in Figure 4.6. The sequence is a football match that starts from almost a static scene with relatively low content. The operating point converges at that point to the lowest spatio-temporal sampling rate (first image). The next operating point transition to a higher sampling rate happens when the players move to their position (second and third images). Once the players are in place, the scene is less active and the camera zooms out getting more spatial details to the scene. At that point, the operating point has higher spatial and lower temporal sampling rates (fourth image). When the play starts, the temporal sampling rate increases rapidly (fifth and sixth images) and settles back down for the rest of the sequence (seventh and eighth images).

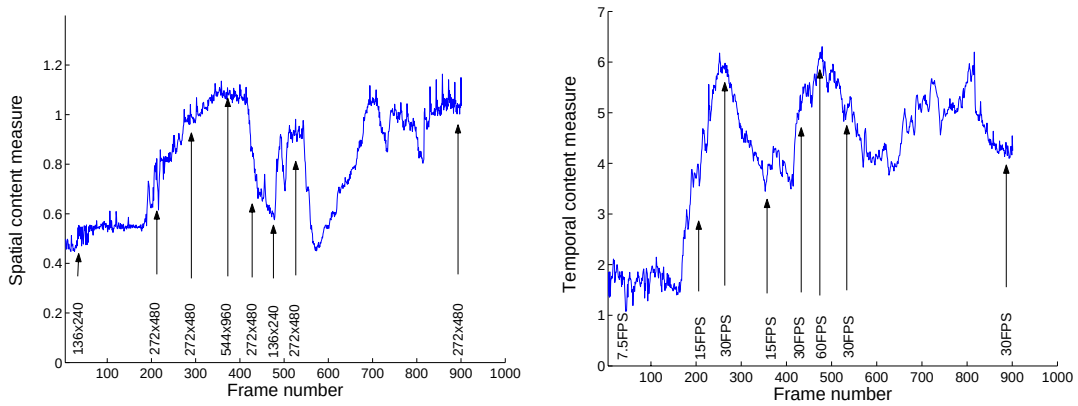

(a) Spatial content measure (b) Temporal content measure

Figure 4.5: Spatial and temporal content measures of the football sequence

Figure 4.6: Input images from the football sequence at the operating point transitions. The numbers below each picture indicate the computed operating points of the closed loop operation.

Chapter 5

Conclusions and future work

In this thesis we have presented a novel approach for image and video sensing. Imaging is done with adaptation to the spatial and temporal content of the scene, optimizing the sensor's sampling rate and the camera transmission or storage bandwidth. We developed a spatial and temporal content measure based on an ℓ_1-norm and characterized it with respect to noise, image bandwidth, and aliasing. Real-time open loop experiment was conducted using an IEEE1394 camera and a PC. The experiment shows the real-time response of the content measures as well as possible dynamics of the operating point. A complete closed-loop system has been simulated using TV high definition video and the results show high correspondence to the scene dynamics and results in significant reduction in the camera output bit-rate.

The output of an adaptive sensor is a sequence of images with varying spatial and temporal sampling rates. This data stream captures the scene more efficiently and with fewer artifacts such that in a post-processing step an enhanced resolution sequence can be composed or lower bandwidth can be used. Having the scene optimally

sampled within the sensor capabilities, the post processing step actually enhance the sequence beyond the sensor operating space. The non-standard stream requires a non-traditional mechanism to address the change in sampling rate. The post processing step can be part of future work in this framework for adaptive imaging.

Well established video processing methods such as super-resolution [8] and motion compensated interpolation [17] are very appropriate for restoring a spatio-temporal high resolution sequence from adaptively captured data. Video super-resolution can take the raw data from the sensor and restore a spatially higher resolution sequence by using data from neighboring frames. Motion compensated interpolation can fill-up the missing frames temporally.

An adaptive sensor system can send additional information to the post-processing engine to allow for an easier, higher quality restoration. This information can include the operating point, a measure for the amount of aliasing, or the content measure itself. In a three sensor configuration, additional information for the motion in the scene can be extracted from the high temporal sampling rate sensor. In systems where compression mechanism such as MPEG encoder already exist, one can think of using the motion estimation and DCT computation as ways to obtain measure of the content and to use it to compute operating point and feed it back to the sensor.

In a complete system where a post-processing stage restores the sequence, a second feedback loop from the post processor to the adaptive sensor can be added. This feedback will use quality measures on the restored sequence and will tune up the adaptive sensor settings to achieve maximum performance. Some of the parameters

that can be tuned include the α, β, and η coefficients of the content measure, conversion curves or look-up tables, temporal or spatial bias in the projection process to the sensor operating space, and the filter gain and behavior in the feedback loop.

The adaptive framework incorporates simple computation that can be implemented as a hardware module within the sensor. In CMOS sensors the adaptive circuit can reside on the same silicon and for CCD devices it can be part of the universal timing generator (UTG) used with any CCD. A possible prototype system for the adaptive sensor can use an existing camera such as the PL-A742 of PixeLink and field programmable gate array (FPGA) for the adaptive circuit and a simple post processing. The output of the system can drive a display directly or stream the raw data to a PC for storage and evaluation.

Appendix A

Simulation environment

In this appendix we present the Matlab simulation environment that was developed for the adaptive image and video sensing. The Matlab routines that are mentioned in the appendix can be retrieved from the Multi-Dimensional Signal Processing research group in the electrical engineering department in the University of California, Santa Cruz. The simulation environment takes as an input raw high definition video data. It creates spatially down sampled sequences at discrete pre-defined resolutions and use them to create the output from the adaptive sensor. The down-sampled video data is processed through the content measures, the operating point computation, and a feedback loop mechanism that defines the next frame to use from the down sampled data at any iteration of the simulation.

High definition source is usually available in MPEG2 program or transport stream formats as it comes through the cables or terrestrial broadcasting. The video sampling rate for high definition is normally 1920×1088 at 60 fields per second (1080i) or 1280×720 at 60 frames per second (720p). Decoding the high definition video to a

raw format and saving it to a local uncompressed binary file can be done using several available tools. In our environment we used the DirectShow graph tool from Microsoft cooperation [18] in conjuction with Mainconcept MPEG splitter and video decoder [16]. Figure A.1 is an example for conversion of transport stream data to a binary file using the DirectShow graph tool.

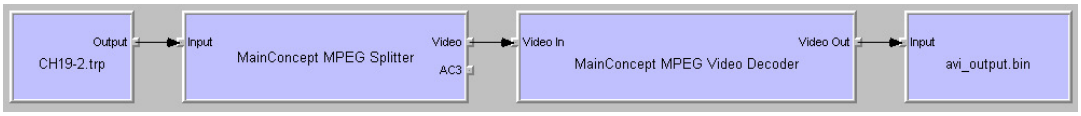

Figure A.1: Example of conversion graph for transport stream data to uncompressed binary

The binary file that is created by the DirectShow graph tool can be read by Matlab using the 'fread' command. Since the simulation is only using the luminance information and the data at the output of the MPEG decoder is formatted as 4:2:2 (the Y component is sampled twice as much as the U and V components in the YUV space) we save only the luminance component of each frame. Each frame is kept in a separate enumerated file to avoid three dimensional matrix size that cannot be processed by Matlab in terms of memory usage. The *HD_capture.m* Matlab routine takes the binary raw video file and converts it to the luminance high definition frames.

Figure A.2 depicts the data preparation stage from the high definition source. To save processing time in the operation of the adaptive sensor, we create spatially down sampled sequences from the raw high definition video data. The spatial down sampling factors are integer numbers only to avoid introduction of interpolation artifact to the video. Using integer down sampling factors limit the simulation to discrete

operating points along the sensor operating space as depicted in Figure 4.4. Temporal down sampling in the operation of the adaptive sensor is done in the closed loop simulation by picking the right frame index from these spatially down sampled sequences. The *HD2sampled_seqs.m* Matlab routine creates the down sampled sequences from the high definition raw video data.

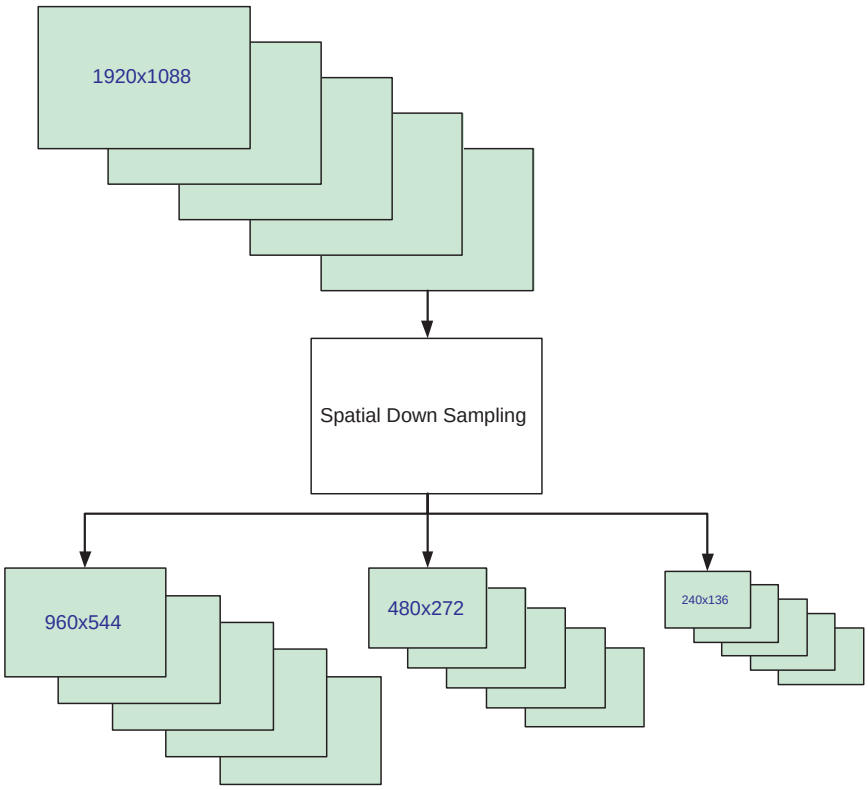

Figure A.2: Sensor operating space preparation from high definition video source

The adaptive sensor simulation uses four spatial operating points and four temporal operating points as created by the down sampling routine. Certain combinations of the spatial and temporal points creates the sensor operating space as depicted in Figure 4.4. The simulation starts at the 480×272, 30 frames per second

operating point. The spatial content measure is performed on each frame using the *L1_spatial_content_measure.m* Matlab routine, with nominal settings of $\alpha = 0.5$ and window size $p = 2$. The temporal content measure is performed on sets of $2p + 1$ frames using the *L1_temporal_content_measure.m* Matlab routine, with nominal settings of $\beta = 0.5$ and window size $p = 2$.

The content measures are converted to required operating point by using look-up tables that were created from the conversion curves as described in Chapter 3. The projection to the sensor operating space is simply done by choosing the nearest point in the space and restricting the change to be no more than one step up or down spatially or temporally. Once the new operating space is found we submit a new frame from the right down sampled sequence at the right time index to the output of the sensor. As a final stage we create an avi file of the adaptive sensor output to evaluate the adapted sequence along with the corresponding content measures presented side by side with the images. This closed loop operation is implemented in the *closed_loop_operation.m* Matlab routine and depicted in Figure A.3.

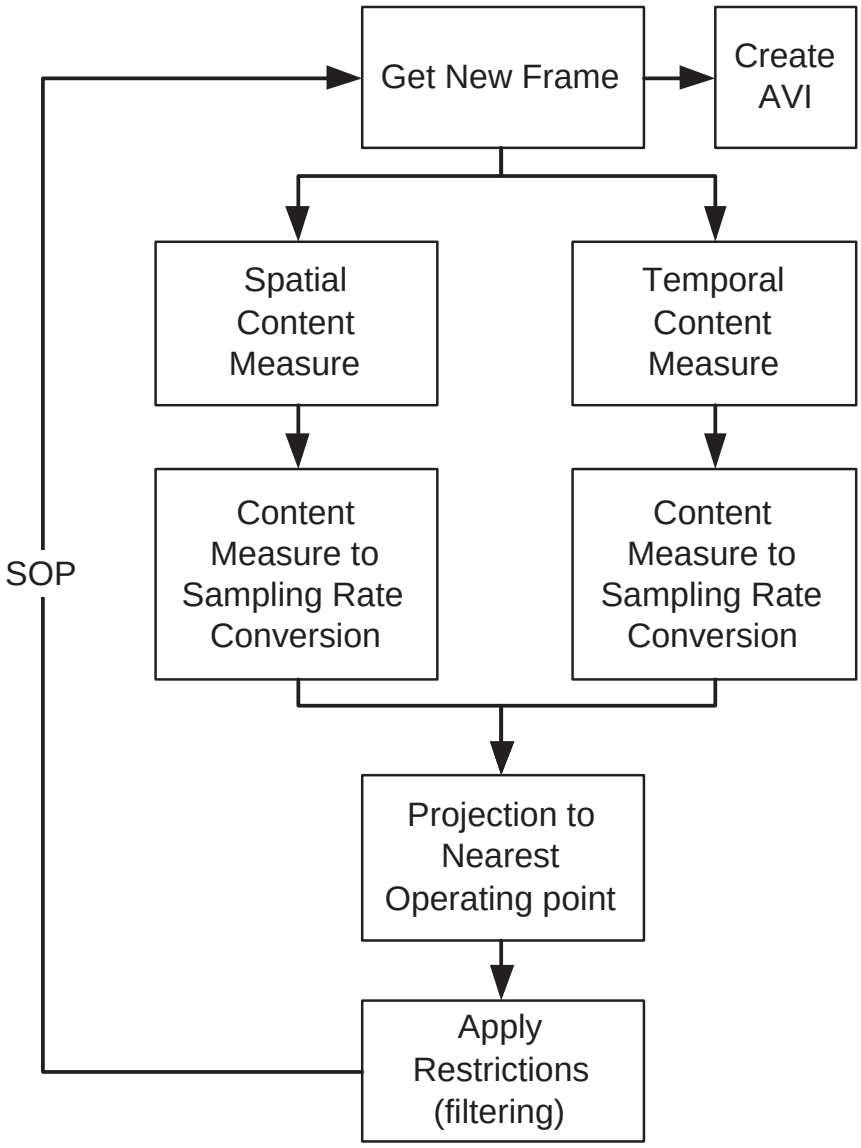

Figure A.3: Block diagram of the closed loop simulation environment

Bibliography

[1] IEEE1394 Trade Association, `http://www.1394ta.org/Technology/Specifications/specifications.htm`.

[2] M. Ben-Ezra and S. K. Nayar, *Motion-based motion deblurring*, IEEE Transactions on Pattern Analysis and Machine Intelligence **26** (2004), no. 6.

[3] Redlake High-Speed Motion Cameras, `http://www.pixelink.com/`.

[4] C.E.Shannon, *A mathematical theory of communication*, Bell Syst. Tech. J. **27** (1948), 379–423, 623–656.

[5] T. Chen, *Digital camera system simulator and applications*, Ph.D. thesis, Stanford University, EE Department, 2003.

[6] CMU 1394 Digital Camera Driver, `http://www-2.cs.cmu.edu/~iwan/1394/`.

[7] M. Elad, *On the bilateral filter and ways to improve it*, IEEE Transactions on Image Processing **11** (2002), no. 10, 1141–1151.

[8] S. Farsiu, D. Robinson, M. Elad, and P. Milanfar, *Fast and robust multi-frame super-resolution*, IEEE Transactions on Image Processing **13** (2004), 1327–1344.

[9] M. Green, *Statistics of images, the tv algorithm of rudin-osher-fatemi for image denoising and an improved denoising algorithm*, UCLA CAM Report (2002), 02–55.

[10] G. E. Healey and R. Kondepudy, *Radiometric ccd camera calibration and noise estimation*, IEEE Transactions on Pattern Analysis and Machine Intelligence **16** (1994), no. 3.

[11] S. Kullback, *Information theory and statistics*, Tech. report, Dover Publications, Inc, 1968.

[12] S. H. Lim, *Video processing applications of high speed cmos sensors*, Ph.D. thesis, Stanford University, EE Department, 2003.

[13] A. Papoulis and S. Unnikrishna Pillai, *Probability, random variables and stochastic processes*, McGraw-Hill, 2001.

[14] E. Shechtman, Y. Caspiand, and M. Irani, *Increasing space-time resolution in video*, Proceedings of the Seventh European Conference in Computer Vision **1** (2002), 753.

[15] H.R. Sheikh and A.C. Bovik, *Image information and visual quality*, Proceedings of the IEEE International Conference on Acoustics, Speech, and Signal Processing **3** (2004), 709–12.

[16] MainConcept Multimedia Technologies, `http://www.mainconcept.com/`.

[17] A. M. Tekalp, *Digital video processing*, Prentice-Hall, 1995.

[18] Microsoft Cooperation DirectShow Graph Tool, `http://msdn.microsoft.com/`.

[19] PixeLink Machine Vision, `http://www.adstech.com/`.

[20] Pyro webcam from ADS tech, `http://www.adstech.com/`.

[21] J. Yang-Peláez and W. C. Flowers, *Information content measures of visual displays*, Proceedings of the IEEE Symposium on Information Vizualization (2000).

[22] H. You, Q. Zhu, and A. Alwan, *Entropy-based variable frame rate analysis of speech signals and its application to asr*, ICASSP, Montreal, Canada (2004).

[23] Q. Zhu and A. Alwan, *On the use of variable frame rate analysis in speech recognition*, ICASSP (2000), 3264–3267.